Journal of Applied Polymer Science

Structure and properties of poly(acrylonitrile-*co*-methyl acrylate) membranes prepared via thermally induced phase separation

Na Han,[1,2,3] Juncheng Xiong,[1,2] Sumei Chen,[1,2] Xingxiang Zhang,[1,2] Yulin Li,[1,2] Linli Tan[1,2]

[1]State Key Laboratory of Separation Membrane and Membrane Process, School of Materials Science and Engineering, Tianjin Polytechnic University, Tianjin 300387, China

[2]Tianjin Municipal Key Lab of Fiber Modification and Functional Fiber, School of Materials Science and Engineering, Tianjin Polytechnic University, Tianjin 300387, China

[3]CHTC HELON CO., Weifang, Shandong 261100, China

Correspondence to: X. Zhang (E-mail: zhangpolyu@aliyun.com)

ABSTRACT: Poly(acrylonitrile-*co*-methyl acrylate) [(P(AN-MA)] microporous membranes were prepared via a thermally induced phase separation (TIPS) process by using γ-butyrolactone (γ-BA) and glyceryl triacetate (GTA) as the mixed diluent. The purpose of this work is to investigate the effects of the γ-BA content, P(AN-MA) concentration, and cooling rate on the structure and properties of P(AN-MA) membranes. A lacy structure with high connectivity was formed with 50 wt % γ-BA, and 50 wt % GTA comprising the mixed diluent. With an increase in the γ-BA content, the pore structure acquires semi-closed or completely closed cell-like morphologies. The different phase separation mechanisms greatly influence the mechanical properties of the P(AN-MA) membranes. P(AN-MA) membranes with a lacy structure possess better tensile strength than those with semi-closed or completely closed cell-like structures. The membrane pore size grows larger when the TIPS process utilizes a higher γ-BA content and a lower cooling rate. © 2016 Wiley Periodicals, Inc. J. Appl. Polym. Sci. **2016**, *133*, 43444.

KEYWORDS: membranes; morphology; phase behavior; separation techniques; thermoplastics

Received 7 October 2015; accepted 18 January 2016

DOI: 10.1002/app.43444

INTRODUCTION

Polyacrylonitrile (PAN) separation membranes have attracted worldwide interest for use in water treatment,[1] pervaporation,[2] enzyme immobilization,[3] and biomedical applications. These materials exhibit superior inherent ultraviolet (UV) and chemical resistances, thermal stability, mechanical properties, and hydrophilicity.[4] Upon heating, adjacent cyano groups in the PAN chains cyclize to form stiff six-membered rings; meanwhile, PAN undergoes a degradation reaction at ~250 °C prior to melting at ~320 °C.[5] Therefore, PAN-based microporous membranes are commonly produced by a nonsolvent induced phase separation (NIPS) method. A series of studies discussing the manufacture PAN membranes have been performed, and most of the membranes were obtained by using chemically modified polyacrylonitrile or physical blends of polyacrylonitrile via NIPS. Asatekin *et al.* have used polyacrylonitrile-*graft*-poly (ethylene oxide) (PAN-*g*-PEO) to prepare nanofiltration (NF) membranes using dimethyl formamide (DMF) as a solvent.[6] Nanofiltration thin film composite (TFC) membranes are based on the microphase separation of the backbone from the side chains of a PAN-*g*-PEO comb copolymer. These membranes exhibited high fouling resistance and high flux.[7] Zheng *et al.* have prepared thermo-responsive PAN membranes by using poly(acrylonitrile-*g*-isopropylacrylamide) as an additive and DMF as the solvent.[8] Qin *et al.* have prepared ultrafiltration membranes from blends of PAN and poly(vinyl pyrrolidone) (PVP); the as-spun fiber membranes were post-treated by hypochlorite solutions with different concentrations.[9] However, NIPS technology requires large amounts of polar, toxic or corrosive solvents, e.g., dimethyl formamide (DMF) or dimethyl sulfoxide (DMSO), to dissolve the high molecular PAN-based polymer, which increases the cost and pollutes the air.

As an alternative to NIPS, the thermally induced phase separation (TIPS) process has been have been applied to many polymers, such as polypropylene,[10] poly(methyl methacrylate),[11] and polyvinylidene fluoride (PVDF).[12,13] In the TIPS process, a polymer is dissolved in a diluent at a temperature that is above its melting point, and by cooling the solution, phase separation is induced. Polymeric porous membranes are then obtained after the diluent is removed by extraction, evaporation or freeze-drying.[14–16] Hence, the heat transfer and the mass transfer across the interface between the polymer solution and the

coagulation bath are both very important for the phase separation process and the ultimate membrane morphology.[17] Compared with NIPS, the TIPS method has several advantages: (1) an absence of macrovoids, (2) better mechanical properties, and (3) a narrower pore size distribution in the resultant membranes, and (4) the possibility of obtaining symmetrical structures.[18–21] The TIPS technique is an effective method to prepare microporous semi-crystalline membranes.[22]

In TIPS, by varying the composition and temperature, the polymer solutions can be brought into three different regions (a region of spinodal decomposition and two regions of nucleation and growth located between the binodal curve and spinodal curve). When the binodal line, which is the border between the homogeneous solution and phase-separated solution, is located above the crystallization temperature, liquid–liquid (L–L) phase separation occurs.[23] The binodal curve and spinodal curve coincide at the critical point. These three different regions represent the three different mass transport mechanisms that can occur during the membrane formation by liquid–liquid phase separation: (i) nucleation and growth of droplets of the polymer-rich phase followed by solidification of the polymer-rich phase, which forms a bead-like membrane structure; (ii) spinodal decomposition into two interconnected phases with subsequent solidification of the polymer-rich phase, which forms a bicontinuous membrane structure; and (iii) nucleation and growth of droplets of the polymer-lean phase followed by solidification of the polymer-rich phase leading to the formation of a cellular structure.[24] However, a few studies have been reported on the preparation of PAN membranes via the TIPS method. Xu *et al.* have manufactured PAN membranes with sheet-, needle-, and cellular-like pores via a TIPS process using dimethyl sulfone (DMSO2) and glycerol as the diluent and the non-solvent additive, respectively.[25] Building on previous research, the same group has manufactured PAN membranes via a TIPS process using polyethylene glycol (PEG) with different molecular weights, which exhibited cellular like pores and high water flux.[26]

In this study, a flexible comonomer, methyl acrylate (MA), was used to synthesize the copolymer poly(acrylonitrile-*co*-methyl acrylate) [P(AN-MA)], which further disrupted the order found in the PAN system, thereby reducing its melting temperature and facilitating the melt processing of the PAN-based copolymer.[27–29] Thus, the self-made melt processable [P(AN-MA)] was used as the polymer matrix, while γ-butyrolactone (γ-BA) and glyceryl triacetate (GTA) served as the diluent and non-solvent additive, respectively; membranes were then fabricated via TIPS. A systematic study was carried out to investigate the effects of the GTA content, P(AN-MA) concentration, and cooling rates on the pore shape, size, and porosity, as well as on the water flux and mechanical properties of the P(AN-MA) microporous membranes.

EXPERIMENTAL

Materials

Poly(acrylonitrile-*co*-methyl acrylate) [P(AN-MA)] was synthesized by emulsion polymerization in our lab[30] (T_m, 150 to ~180 °C; T_d, 317 to ~325 °C). γ-Butyrolactone (γ-BA, 98%) and glyceryl triacetate (GTA, 98%)were purchased from Tianjin Guangfu Fine Chemical Institute. Ethanol and hexane were obtained from Tianjin Fengchuan Chemical Reagent Science and Technology Co. The P(AN-MA) copolymer was dried before use, and the other chemicals were used without further purification.

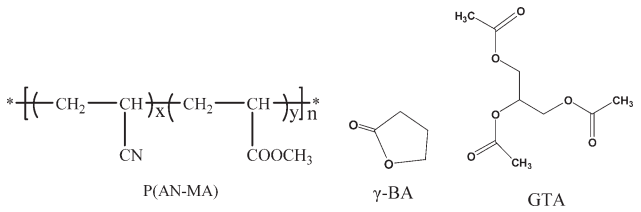

Figure 1. Chemical structure of P(AN-MA), γ-BA, and GTA.

Membrane Preparation

The P(AN-MA)/γ-BA/GTA mixture was heated at 180 °C in a nitrogen atmosphere until a homogeneous solution was achieved. After degassing air bubbles at 180 °C, the solution was quickly poured onto a clean glass mold (sheet thickness ~3 cm), which was preheated in an oven at 180 °C. Afterwards, the samples together with molds were immediately immersed in a cooling bath (water bath at 0 °C or 30 °C, air bath at −4 °C). One hour later, the as-prepared membranes solidified and were removed from the mold. The diluent was removed by immersing the film in ethanol over 24 h at room temperature (25 °C). The final porous membranes were saved in deionized water for further characterization. The chemical structure of raw materials are shown in Figure 1. The specific experimental details are listed in Table I. The samples are denoted as xP(yBzG), where P, B, and G represent P(AN-MA), γ-BA, and GTA and x, y, and z represent the respective mass fractions. To avoid the collapse of the pores during drying, the wet membrane was washed sequentially with ethanol and hexane. Then, the membrane was dried in a vacuum oven for 24 h at 40 °C.

Scanning Electron Microscopy (SEM) Observation

Field-emission scanning electron microscopy (FESEM, Hitachi S-4800, Hitachi, Japan) was employed to observe the membrane cross-section and surface morphologies. To obtain a flat cross-section, the membranes were frozen by liquid nitrogen and fractured. After the samples were coated with gold using an SCD-005 sputter coater, the cross-section, top and bottom surfaces were imaged by FESEM at an acceleration voltage of 5.0–10.0 kV.

Pore Size and Porosity Determination

The average pore diameters in each membrane were determined by image analysis software that relied on scanning electron microscopic (SEM) images of the P(AN-MA) membrane cross-sections. The method for measuring the pore size has been reported in the literature.[31] Porosity is defined as the volume of pores divided by the total volume of membrane.[32] A wet P(AN-MA) membrane was weighed immediately after removing the superficial water with filter paper. Then, the wet membrane was dried in the manner described in "Membrane preparation." Each sample was tested at least three times. The porosity (P) was calculated according to the following formula:

$$P = \frac{(w_0 - w_1)/\rho_{water}}{w_0 - w_1/\rho_{water} + w_1/\rho_{P(AN\text{-}MA)}} \times 100\% \quad (1)$$

where w_0 is the wet membrane weight, w_1 is the dry membrane weight, and ρ_{water} and $\rho_{P(AN\text{-}MA)}$ are the densities of water and P(AN-MA), respectively.

Table I. Preparation Conditions of P(AN-MA) Membranes and Average Pore Size

Sample No.	Sample	P(AN-MA) concentration (wt %)	BA content in the mixed diluent (wt %)	GTA content in the mixed diluent (wt %)	Cooling bath (°C)	Average pore size (μm)
1	15P(50B50G)	15	50	50	−4[a]	0.4 ± 0.3
2					0[b]	0.7 ± 0.4
3					30[b]	0.8 ± 0.3
4	15P(60B40G)	15	60	40	−4[a]	1.8 ± 0.9
5					0[b]	1.2 ± 0.6
6					30[b]	2.0 ± 1.0
7	15P(70B30G)	15	70	30	−4[a]	1.2 ± 0.8
8					0[b]	1.0 ± 0.8
9					30[b]	1.6 ± 0.7
10	18P(50B50G)	18	50	50	−4[a]	0.3 ± 0.1
11					0[b]	0.4 ± 0.2
12					30[b]	0.8 ± 0.4
13	18P(60B40G)	18	60	40	−4[a]	1.4 ± 0.8
14					0[b]	0.7 ± 0.4
15					30[b]	1.5 ± 0.6
16	20P(50B50G)	20	50	50	−4[a]	0.2 ± 0.1
17					0[b]	0.4 ± 0.3
18					30[b]	1.2 ± 0.7
19	20P(60B40G)	20	60	40	−4[a]	0.9 ± 0.6
20					0[b]	0.8 ± 0.5
21					30[b]	1.1 ± 0.8

[a] Air bath.
[b] Water bath.

Pure Water Flux Measurement

The water flux of membranes (surface area is 18 cm^2) was determined on a homemade device with a pressure-driven test cell. The membranes were first pre-pressurized at 0.12 MPa at 25 °C for 30 min. Then, the pressure was reduced to 0.10 MPa for operation at a steady-state water flux with less than 2% deviation. Each sample was tested in at least three parallel experiments, and the average was taken as the final value. The pure water flux (J_W) was defined by the following formula:

$$J_W = \frac{V}{A \times \Delta t} \quad (2)$$

where J_W is the pure water flux (L/m^2 h), V is the permeate volume (L), A is the membrane area (m^2), and Δt is the permeate time (h).

Tensile Strength and Elongation at Break

The tensile strength and elongation at break of the membrane samples were determined by a universal testing machine (CMT4503, Meitesi Industry Co., China). The samples were cut into rectangle shapes with a gauge length of 40 mm and a width of 10 mm. The test was carried out at a strain rate of 10 mm/min at 25 °C. The membrane was fixed vertically between two pairs of clamps with a test length of 20 mm. The thickness was measured by an electronic digital readout micrometer (0–25 mm/0.001, Shanghai Zijiu Measuring Tool Co., China), and the mechanical values are shown in Figure 7. The reported values represent the average of at least eight samples.

RESULTS AND DISCUSSION

Effects of the γ-BA Content on the Membrane Structure

The P(AN-MA) copolymer possessed a high polar force due to the cyano side group (–CN). The P(AN-MA) membranes solidified as soon as they contacted with the water bath at a lower temperature. The dense top and bottom surfaces of the P(AN-MA) membrane tended to form upon quenching. Therefore, this study primarily focuses on the cross-sectional data. Figure 2 shows the cross-section morphologies of the P(AN-MA) membranes prepared from the ternary system with various amounts of γ-BA in the mixed diluent and at different cooling bath temperatures.

When the γ-BA content was 50 wt % in the mixed diluent, the cross-section structures of the membranes were branch-like and showed good connectivity between pores, which are typically derived from spinodal phase separation. These data also indicated that the ternary system tended to follow a spinodal phase separation and when the cooling bath temperature was between −4 and 30 °C, irrespective of the cooling mediums with different thermal coefficient. As the γ-BA content increases to 60 wt %, the branch-like porous morphology completely disappears, and semi-closed elliptic pores can be observed. It indicates that the phase separation mechanism changes from spinodal phase

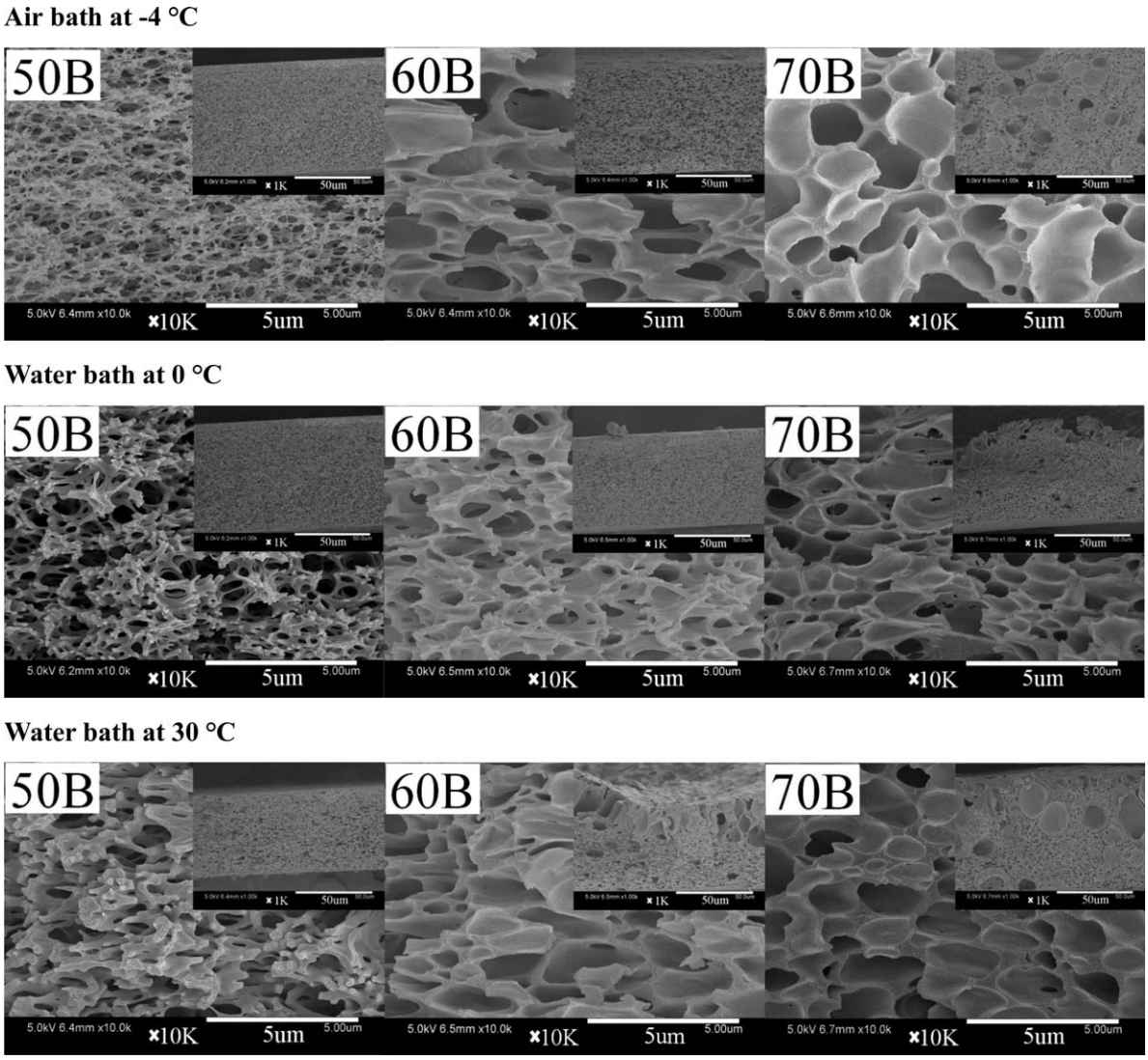

Figure 2. SEM images of the cross-sections (10K×) of membranes prepared from 15 wt % P(AN-MA). The membranes were prepared from a ternary system with 50 wt % γ-BA (50B), 60 wt % γ-BA (60B), and 70 wt % γ-BA (70B) at different cooling bath temperatures.

separation to nucleation-and-growth. When the γ-BA content reaches 70 wt %, the irregular elliptic pores had a tendency to turn into a more circular shape. It is notable that the cellular structure contained almost no semi-closed cell-like pores when 70 wt % γ-BA was used in the mixed diluent.

As γ-BA dissolves the P(AN-MA), a lower content of this solvent in the ternary mixture leads to a weaker interaction between the copolymer and the mixed diluent. Tiny thermal or concentration fluctuations are sufficient to produce a thermodynamically unstable solvent rich phase. The typical situation of demixing is constituted of droplets of one phase dispersed in a continuous matrix of the other phase. In the process of spinodal phase separation, both phases are formed and grow simultaneously. A branched structure with good connectivity was finally formed in order to reduce the interface area between phases.

As the γ-BA content increases to 60 wt %, the miscibility of diluents and P(AN-MA) was improved. Semi-closed cell-like structures could be re-formed due to the fast cooling rate that depressed the growth of droplets. When the γ-BA content is at 70 wt %, interactions between the polymer and the diluents increased further and a completely closed cell-like structure appears after the cooling process.

The average pore size of the P(AN-MA) membranes is 0.4–2.0 μm (pore diameters are listed in Table I). As the γ-BA content increases from 60 wt % to 70 wt %, the average pore size of the membrane that was quenched in the air bath decreases from 1.8 μm to 1.2 μm. For the microporous membranes obtained in the water baths at 0 °C and 30 °C, the pore sizes decrease from 1.2 μm to 1.0 μm and 2.0 μm to 1.6 μm, respectively. The pore size results and the SEM data revealed that it is possible to control the membrane formation process and structure by altering the ratio between the blend and diluent solvents employed in the TIPS process.

Effect of P(AN-MA) Concentration on the Membrane Structure

The ternary systems with a 50 wt % γ-BA content in the mixed diluent were chosen as representative samples. The effects of the

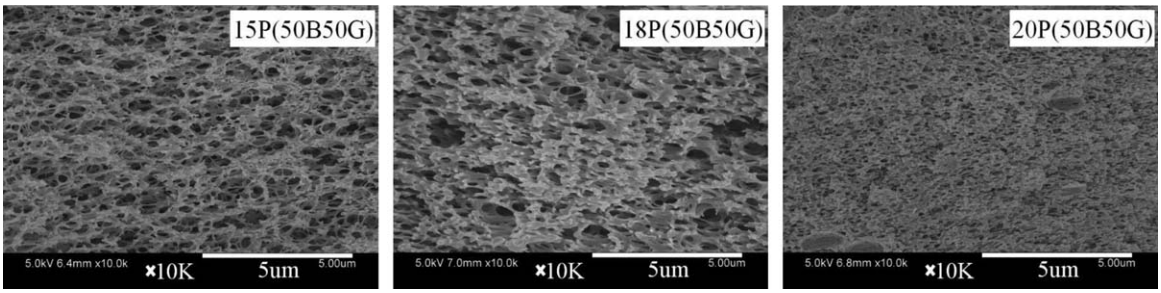

Figure 3. SEM images of the cross-sections (10K×) of membranes prepared from 15 wt % to 20 wt % P(AN-MA). The membranes were prepared from the ternary system with 50 wt % γ-BA in the mixed diluent and an air bath at −4 °C.

P(AN-MA) concentration on the morphology of the membrane cross-section were investigated as the P(AN-MA) concentration was increased from 15 wt % to 20 wt %. Figures 3 and [4] show the cross-section of P(AN-MA) membranes that were quenched in an air bath (−4 °C) and a water bath (0 °C), respectively. It is observed that the structure of the cross-section converted from branch-like to cell-like with increasing amounts of P(AN-MA). Meanwhile, the average pore size of the membrane formed in the air bath at −4 °C was reduced from 0.4 μm to 0.2 μm (Figure 4), whereas, the pore size of those formed in the 0 °C water bath decreased from 0.7 μm to 0.4 μm. It implies that the pore structure formed via spinodal phase separation as the concentration of P(AN-MA) copolymer is 15 wt %. With P(AN-MA) concentrations increasing, in other words, the concentration of P(AN-MA) is higher than 15 wt %, the phase separation mechanism changes from spinodal phase separation to nucleation-and-growth. Meanwhile, the viscosity of copolymer and diluents system increase, the growth of droplets is restricted. According to Ostwald ripening,[33] congealing,[34] and coalescence mechanisms,[35] entanglements between copolymer chains occur during film-formation, and with more and more P(AN-MA) content available, the membrane morphology finally results in a cell-like structure and with a smaller pore size.

Effect of the Cooling Rate on the Membrane Structure

Figure 5 shows the SEM cross-section images of the P(AN-MA) membranes prepared in a water bath at different temperatures. It is found that the micropores in the cross-section show elliptical shapes even though no additional outer forces were exerted. When quenched in the 0 °C water bath, the pores presented a semi-closed cell-like structure. However, the pores were almost completely closed as the water bath temperature increased to 30 °C, which was ascribed to the intensifying macromolecular movement that accompanied the increase in water temperature. Therefore, the casting solution solidified at a higher speed in the 30 °C water bath, which suppressed liquid–liquid phase separation. Meanwhile, a lower curing rate leads to the formation of pure liquid and polymer phases in the system, and the pore size also increases with the water bath temperature (Table I). This result is associated with a longer growth time for liquid droplets at lower cooling rates that are induced by higher environmental temperatures.[25,36] The membranes [15P(60B40G) and 20P(60B40G)] quenched in a water bath at 30 °C have pore sizes approximately 2.0 μm and 1.1 μm, which are larger than pores obtained at 0 °C in a water bath (∼1.2 μm and ∼0.8 μm). Zhang et al. have reported that droplet growth mainly depends on the viscosity of the solution.[37,38] In our experiments, a slightly higher P(AN-MA) concentration dramatically increases the viscosity of the ternary mixture. Therefore, it is observed that the 20P(60B40G) membrane possesses pores sizes that are more resistant to change due to the high viscosity of casting solution.

Water Flux and Porosity of P(AN-MA) Membranes

The water permeability of the P(AN-MA) membranes was altered significantly by changing the cooling bath temperature, γ-BA concentration or P(AN-MA) concentration. The water flux and porosity of P(AN-MA) membranes that were prepared under different conditions are shown in Figures 6 and 7. In general, as the temperature of the water bath increases from 0 °C to 30 °C, the water flux decreases. This trend is associated with the dense skin layer that forms when the casting solution was quenched at a lower cooling rate and is consistent with the structure of the cross-section (as Figure 5).

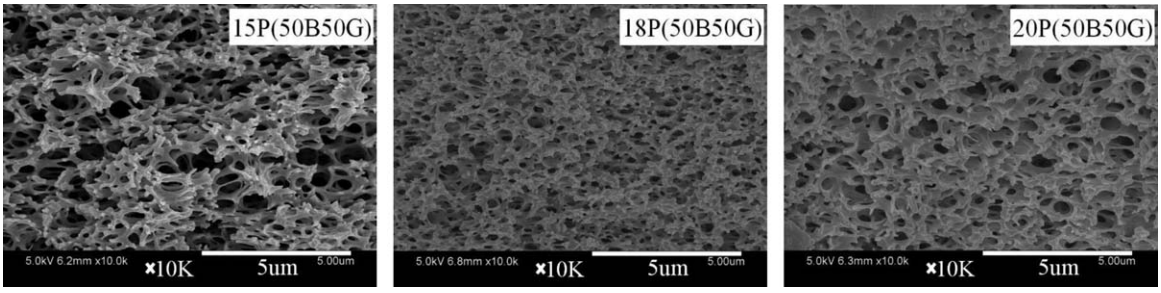

Figure 4. SEM images of the cross-sections (10K×) of membranes prepared from 15 wt % to 20 wt % AN-MA. The membranes were prepared from the ternary system with 50 wt % γ-BA in the mixed diluent and a water bath at 0 °C.

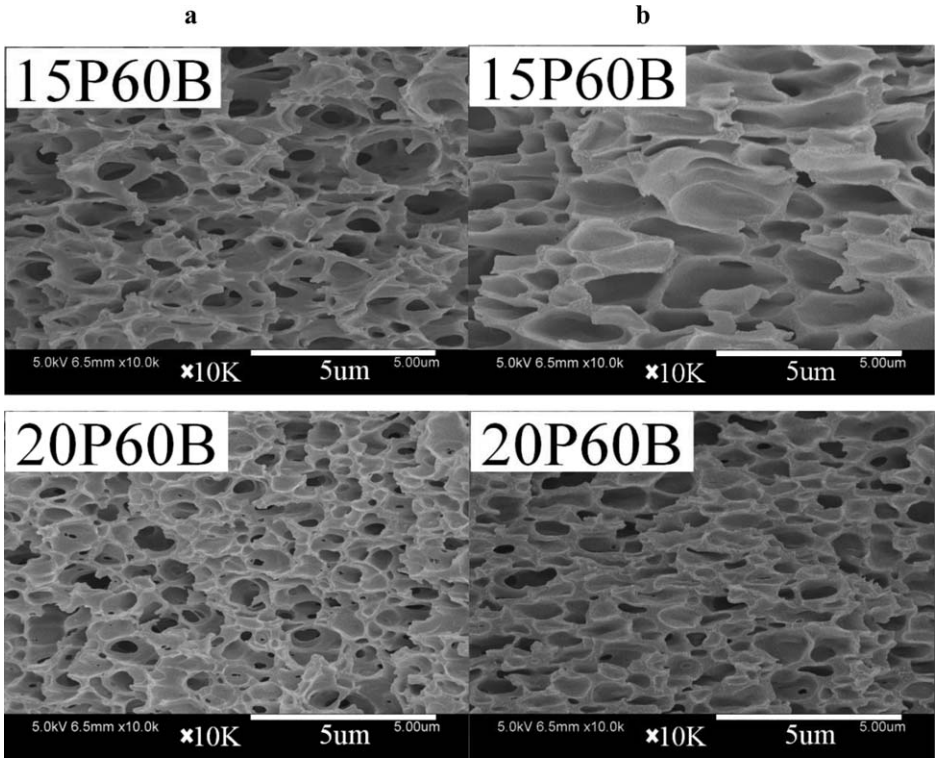

Figure 5. SEM images of cross-sections (10K×) of membranes prepared in different cooling baths: (a) prepared in a water bath at 0 °C and (b) in a water bath at 30 °C.

It can be observed from Figure 7 that the P(AN-MA) membrane fabricated at −4 °C in the air bath has a higher water flux than those obtained in water baths. The 15P(50B50G) membrane that formed by cooling in the −4 °C air bath exhibits the maximum water flux (~80 L/m^2 h).

As observed in Figures 6 and [7], the porosity of membranes prepared from different P(AN-MA) concentration changes little, which implies that the P(AN-MA) concentration has little effect on porosity in this study. It can be observed that the P(AN-MA) membrane prepared from 50 wt % γ-BA in the mixed diluent had a higher water permeability than those prepared from 60 wt % and 70 wt % γ-BA content; however, the porosity and mean pore size of this membrane were lower than those of the latter ones. The porous structure of the 50 wt % γ-BA membrane is branch-like and highly interconnected. However, the connectivity of pores are reduced with an increase in either γ-BA content or P(AN-MA) concentration (Figure 3). In addition, the surface structure has a significant impact on the permeability of porous membranes.

The surface of P(AN-MA) membranes solidified as soon as the casting solution was quenched by the cooling bath. Dense

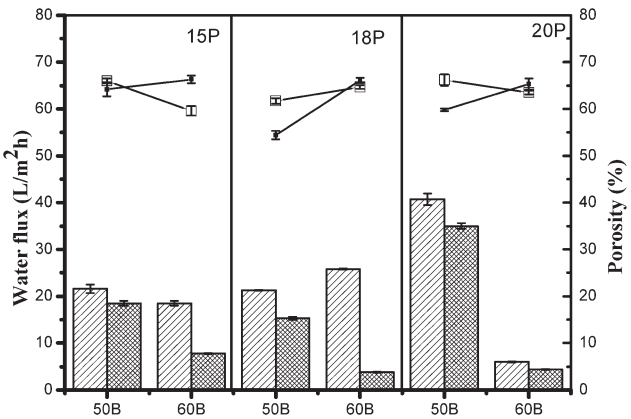

Figure 6. Water flux (bars) and porosity (squares) of P(AN-MA) membranes prepared with different cooling rates. The bars with diagonal lines and clathrate bars represent water flux in water baths at 0 °C and 30 °C, respectively. The hollow and solid squares represent porosity in water baths at 0 °C and 30 °C, respectively.

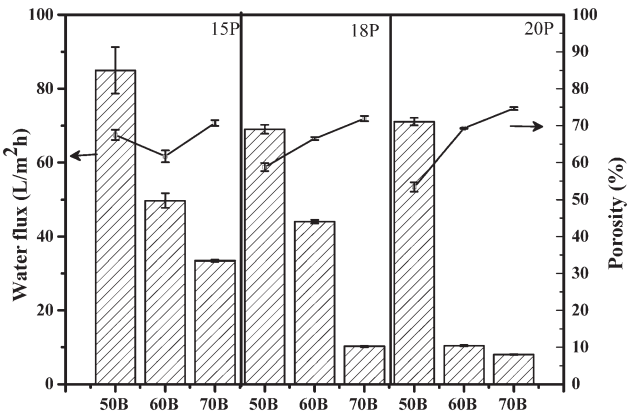

Figure 7. Water flux (bars) and porosity (squares) of P(AN-MA) membranes prepared in an air bath at −4 °C.

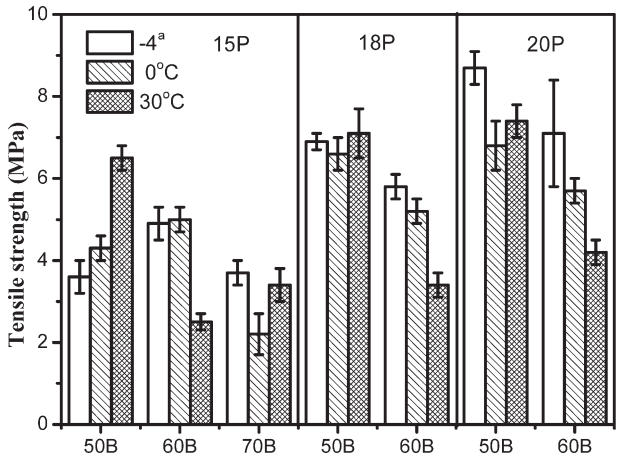

Figure 8. Tensile strength of the P(AN-MA) membranes.

surfaces on the top and bottom of the membrane promptly formed as the polar P(AN-MA) copolymer chains were maintained contact with water. Second, liquid droplet growth was prevented by the solidification of P(AN-MA) that accompanied the decreasing temperature of the ternary system, which lead to lower connectivity and permeability in the resultant membrane. Thus, it is critical for future research to delay the solidification of P(AN-MA) during the TIPS process.

Mechanical Properties of P(AN-MA) Membranes

The mechanical properties of membranes are crucial to their practical applications. Figure 8 displays the tensile strength of P(AN-MA) membranes, and it is observed that the tensile strength increases with P(AN-MA) concentration. This is associated with a more compact arrangement of entangled P(AN-MA) macromolecules. The tensile strengths of the P(AN-MA) membranes prepared under different conditions ranged from 2.2 MPa to ~8.7 MPa, and the 20P(50B50G) membrane prepared in an air bath at −4 °C had the highest tensile strength of 8.7 MPa. In particular, the membranes that were fabricated from 50 wt % γ-BA possessed preferable tensile strengths due to the extensive connectivity evident from their cross-sections. The branch-like structure has a high binding force when compared with the semi-closed cell-like structure. Eventually, the membranes with branch-like pores break in a ductile fashion, while those with semi-closed or fully closed cell-like structures break in a brittle fashion. As mentioned above, the reduction in mechanical properties of P(AN-MA) membranes prepared from higher γ-BA content was due to the lower connectivity of membrane pores with semi-closed or completely closed cells.

It is shown that membranes quenched in a water bath at 30 °C exhibit less elongation than those quenched in a 0 °C water bath. This is ascribed to the dense surface structures of membranes quenched in cooling baths at a higher temperature, which accelerates macromolecular movement and solidification. Thus, strain-hardening and lower elongation appears. In addition, the membrane obtained in the air bath has the maximum value of elongation, which is derived from its highly connected branch-like structures. Moreover, it is also found that the elongation percentage of a membrane decreases with the P(AN-MA) concentration or with the increasing γ-BA content, which is also associated with dense surfaces. It is suggested that the P(AN-MA) concentration and γ-BA content should be adjusted according to the practical requirements regarding tensile strength or elongation. Additionally, the cooling bath and the cooling rate are crucial for improving the connectivity, permeability, and mechanical properties of P(AN-MA) membranes, which will be further discussed in future work.

CONCLUSIONS

Poly(acrylonitrile-*co*-methyl acrylate) membranes were successfully fabricated via a thermally induced phase separation process using γ-butyrolactone and glyceryl triacetate for the mixed diluent. The branched structure and semi-closed or completely closed cell-like structure were obtained with a 50–70 wt % γ-BA content. The change in pore structure was due to the different thermodynamically driven mechanisms at work during the initial stage of the phase separation. A high γ-butyrolactone/glyceryl triacetate ratio, a suitable poly(acrylonitrile-*co*-methyl acrylate) concentration and a fast cooling rate were more likely to result in phase separation that followed a spinodal decomposition mechanism, which resulted in a branched structure with high connectivity; conversely, when the phase separation was based on a nucleation-growth mechanism, semi-closed or completely closed cell-like structures were obtained throughout the membrane. Moreover, membranes with branch-like structures possessed better tensile strength than those with semi-closed or completely closed cell-like structures. Further exploration of the dense surface structure that was observed for poly(acrylonitrile-*co*-methyl acrylate) membranes is in progress, and these experiments are expected to be useful in optimizing the permeability and mechanical properties for different poly(acrylonitrile-*co*-methyl acrylate) membrane applications.

ACKNOWLEDGMENTS

The authors wish to thank the National Natural Science Foundation of China (21206123); Doctoral Program of Higher Education of China (20111201120001); China Postdoctoral Science Foundation (2014M551026); Basic Application and Frontier Project of Tianjin Municipal (13JCQNJC02300) and the Innovation Fund Designated for postdoc of Shandong Province (201402011) for financial support.

REFERENCES

1. Vasileva, N.; Godjevargova, T.; Ivanova, D.; Gabrovska, K. *Int. J. Biol. Macromol.* **2009**, *44*, 192.
2. Azari, S.; Karimi, M.; Kish, M. H. *Chemres* **2010**, *49*, 2442.
3. Wang, Z. G.; Wan, L. S.; Xu, Z. K. *J. Membr. Sci.* **2007**, *304*, 8.
4. Junga, B.; Yoona, J. K.; Kima, B.; Rheeb, H. W. *J. Membr. Sci.* **2005**, *246*, 67.
5. Korte, S. Wiley Database of Polymer Properties; Wiley & Sons: New York, **1999**.
6. Asatekina, A.; Kangb, S.; Elimelechb, M.; Mayesc, A. M. *J. Membr. Sci.* **2007**, *298*, 136.

7. Asatekin, A.; Olivetti, E. A.; Mayes, A. M. *J. Membr. Sci.* **2009**, *332*, 6.
8. Fei, Z. D.; Wan, L. S.; Wang, W. M.; Zhong, M. Q.; Xu, Z. K. *J. Membr. Sci.* **2013**, *432*, 42.
9. Qin, J. J.; Cao, Y. M.; Li, Y. Q.; Li, Y.; Oo, M. H.; Lee, H. *Sep. Pyrif. Technol.* **2004**, *36*, 149.
10. Lloyd, D. R.; Kim, S. S.; Kinzer, K. E. *J. Membr. Sci.* **1991**, *64*, 1.
11. Yoneda, S.; Han, W.; Hasegawa, U.; Uyama, H. *Polymer* **2014**, *55*, 3212.
12. Liang, H. Q.; Wu, Q. Y.; Wan, L. S.; Huang, X. J.; Xu, Z. K. *J. Membr. Sci.* **2014**, *465*, 56.
13. Ma, T.; Cui, Z. Y.; Wu, Y.; Qin, S.; Wang, H.; Yan, F.; Han, N.; Li, J. *J. Membr. Sci.* **2013**, *444*, 213.
14. Tang, Y. H.; He, Y. D.; Wang, X. L. *J. Membr. Sci.* **2015**, 474.
15. Lloyd, D.; Kinzer, K.; Tseng, H. S. *J. Membr. Sci.* **1990**, *52*, 239.
16. Matsuyama, H.; Berghmans, S.; Lloyd, D. R. *Polymer* **1999**, *40*, 2289.
17. Matsuyama, H.; Yuasa, M.; Kitamura, Y.; Teramoto, M.; Lloyd, D. R. *J. Membr. Sci.* **2000**, *179*, 91.
18. Gu, M. H.; Zhang, J.; Wang, X. L. *J. Appl. Polym. Sci.* **2006**, *102*, 3714.
19. Cui, Z. Y.; Du, C. H.; Xu, Y. Y. *J. Appl. Polym. Sci.* **2007**, *108*, 272.
20. Lin, Y. K.; Tang, Y. H.; Ma, H. Y. *J. Appl. Polym. Sci.* **2009**, *114*, 1523.
21. Yang, J.; Li, D. W.; Lin, Y. K. *J. Appl. Polym. Sci.* **2008**, *110*, 341.
22. Sung, S. K.; Yeom, M. O.; Cho, I. S. *Membr. Form. Modif. Am. Chem Soc.* **1999**, *744*, 42.
23. Matsuyama, H.; Teramoto, M.; Kudari, S.; Kitamura, Y. *J. Appl. Polym. Sci.* **2001**, *82*, 169.
24. Cha, B. J.; Char, K.; Kim, J. J.; Kim, S. S.; Kim, C. K. *J. Membr. Sci.* **1995**, *108*, 219.
25. Wu, Q. Y.; Wan, L. S.; Xu, Z. K. *J. Membr. Sci.* **2012**, *409–410*, 355.
26. Wu, Q. Y.; Liu, B. T.; Li, M.; Wan, L. S.; Xu, Z. K. *J. Membr. Sci.* **2013**, *437*, 227.
27. Han, N.; Zhang, X. X.; Wang, X. C. *J. Appl. Polym. Sci.* **2007**, *103*, 2776.
28. Han, N.; Zhang, X. X.; Wang, X. C. *Iran. Polym. J.* **2010**, *19*, 243.
29. Bhanu, V. A.; Rangarajan, P.; Wiles, K.; Bortner, M.; Sankarpandian, M.; Godshall, D.; Glass, T. E.; Banthia, A. K.; Yang, J.; Wilkes, G.; Wilkes, D.; McGrath, J. E. *Polymer* **2002**, *43*, 4841.
30. Han, N.; Zhang, X. X.; Yu, W. Y.; Gao, X. Y. *Macromol. Res.* **2010**, *18*, 1060.
31. Ji, G. L.; Zhu, L. P.; Zhu, B. K.; C.-F. Zhang, C. F.; Xu, Y. Y. *J. Membr. Sci.* **2008**, *319*, 264.
32. Kamide, K.; Iijima, H.; Matsuda, S. *Polym. J.* **1993**, *25*, 1113.
33. McGuire, K. S.; Laxminarayan, A.; Martula, D. S.; Martula, D.; Lloyd, R. *J. Colloid Interface Sci.* **1996**, *182*, 46.
34. Yiantsios, S. G.; Davis, R. H. *J. Colloid. Interface Sci.* **1991**, *144*, 412.
35. Lifshitz, I. M.; Slyozov, V. V. *J. Phys. Chem. Solids* **1961**, *19*, 35.
36. Cahn, W. J. *Trans. Metall. Soc. AIME* **1968**, *242*, 166.
37. Zhang, C. F.; Bai, Y. X.; Sun, Y. P.; Gu, J.; Xu, Y. Y. *J. Membr. Sci.* **2010**, *365*, 216.
38. Qiu, Y. R.; Matsuyama, H.; Gao, G. Y.; Ou, Y. W.; Miao, C. *J. Membr. Sci.* **2009**, *338*, 128.